Research Article

Qiang Zeng, Jianli Li*, Yue Yu, and Hangyu Zhu*

Effect of Cooling Rate on Crystallization Behavior of $CaO\text{-}SiO_2\text{-}MgO\text{-}Cr_2O_3$ Based Slag

https://doi.org/10.1515/htmp-2020-0023
Received Nov 14, 2019; accepted Dec 03, 2019

Abstract: In order to improve the recycling efficiency of stainless-steel slag resources, the effect of different cooling rates on the crystallization behavior of $CaO\text{-}SiO_2\text{-}MgO\text{-}Cr_2O_3$ based system was studied by using FactSage 7.1, XRD, SEM and IPP 6.0. The results indicated that the spinel is a high-temperature precipitated phase and the cooling rate had less effect on the final grain size of spinel crystals, but had greater influences on the nucleation of spinel crystals and the crystallization of silicates such as α-C2S. When the cooling rate was 12°C/min, the spinel crystals was the unique precipitation. However, the spinel crystals and α-C2S could produce during the slag cooling process as the cooling rate was 1°C/min. Chromium in silicate phase is inclinable to leaching with the dissolution of silicate phase, so the formation of silicate phase should be controlled. According to the influence of the cooling rate on the formation of spinel crystals and the erosion of spinel crystals by α-C2S, it is suggested that the cooling rate of the stainless-steel slag in industrial treatment should not be lower than 12°C/min.

Keywords: stainless-steel slag; cooling rate; spinel crystals; nucleation; hexavalent chromium

1 Introduction

The main components of stainless-steel slag (SS slag) are silicates, which can be applied as raw materials for cement, roadbed, glass-ceramics and other materials. Rosales *et al.* [1] investigated the reaction characteristics about the cementation and pozzolanic for SS slag, and estimated the intensity activity index and its influence on environment. The study showed that the SS slag replaced part of raw materials to produce cement, the economic effect of SS slag could be improved by qualified product indicators. As for Zong *et al.* [2], the DAT curve was determined to compare the composition of SS slag and ceramic paste firstly, and then $CaO\text{-}SiO_2\text{-}MgO$ type ceramic with high added value conforming to national standards in China was produced by mixing SS slag and chemical reagents. However, if SS slag tailings are directly utilized, there is a leaching risk of hexavalent chromium. The leaching toxicity of chromium in cement and cement composites containing chromium was studied. It was found that the content of hexavalent chromium in hydrochloric acid was the highest, and the leaching toxicity of chromium in cement was 55%-80% higher than that of cement composites [3]. Furthermore, it is generally believed that hexavalent is a heavy metal ion, which can easily induce human cancer and affect crop growth [4, 5].

Researchers around the world are interested in solving the leaching of chromium [6–8]. Their researches focused on reducing the leaching of chromium in two directions. One direction was to reduce Cr^{6+} to Cr^{3+} or metal chromium [9]. Adamczyk *et al.* [10] recovered chromium from AOD slag by adding reductant with a chromium recovery rate was 97%. This method could effectively reduce the leaching of chromium. However, the addition of reductant increased the side reaction and affect the subsequent optimization of slag composition, and the economic benefit depended on the content of chromium and its alloys in the slag. Although the yield of chromium could reach 99% by reducing the SS slag with aluminum, the application of industrial conditions was still arduous [11]. The other direction was to solidify chromium in a matrix, spinel crystal phase, or solid material. Sheen *et al.* [12] found that SS

***Corresponding Author: Jianli Li:** The State Key Laboratory of Refractories and Metallurgy, Wuhan University of Science and Technology, Wuhan 430081, China; Hubei Provincial Key Laboratory for New Processes of Ironmaking and Steelmaking, Wuhan University of Science and Technology, Wuhan 430081, China; Key Laboratory for Ferrous Metallurgy and Resources Utilization of Ministry of Education, Wuhan University of Science and Technology, Wuhan 430081, China; Email: jli@wust.edu.cn
***Corresponding Author: Hangyu Zhu:** The State Key Laboratory of Refractories and Metallurgy, Wuhan University of Science and Technology, Wuhan 430081, China; Email: zhuhy@wust.edu.cn
Qiang Zeng, Yue Yu: The State Key Laboratory of Refractories and Metallurgy, Wuhan University of Science and Technology, Wuhan 430081, China

slag replaced cement as concrete bonding material without heavy metal dissolution. It reduced the demand for cement and contributed to the recycling of resources and environmental protection. Previous work showed that the leaching of chromium could be effectively controlled by changing the mineral phase composition of the slag [13]. The main component of spinel phase is Mg (Cr, Al, Fe) $_2O_4$, which was stable in nature. Promoting the formation of more spinel phases, increasing the enrichment of Cr in spinel phases and reducing the leaching toxicity of chromium are the key technical routes in routes in the utilization of SS slag resources [14]. The studies of promoting the formation of spinel crystals were to increase the enrichment of chromium. Although spinel crystal was stable, the edge of spinel crystals eroded in the presence of oxygen and α-C2S [15]. In order to reduce the erosion of spinel crystals, the production of α-C2S should be avoided in the treatment of SS slag, and the growth of spinel crystal should be enhanced [16].

The cooling rate is one of the most important parameters affecting the formation of spinel crystals and the distribution of chromium. The mineralogy and hydraulic properties of synthetic SS slag in two different cooling type, melt spinning granulation or quenching in water. The stabilized slags composed of layered b-C2S, merwinite and bredigite [17]. The volume of SS slag was stable and could be used to make hydraulic binder. The SS slag under different cooling regime was studied by Li and Xue [18]. The investigation showed that cooling rate had a great influence on the migration of chromium. On basic of the decrease of cooling rate, the size of spinel increased correspondingly, the chromium content decrease, and the enrichment rate increased. During the melt solidification process, the nucleus formation rate tends to low temperature, while the nucleus growth rate tends to melt temperature (high temperature), that is, there is an appropriate crystallization region between them. Hence, the effect of different cooling rates on the crystallization behavior of CaO-SiO_2-MgO-Cr_2O_3 based system containing FeO will be discussed in this paper. Moreover, the optimum cooling rate for spinel crystal formation was determined to provide some suggestions for industrialized treatment of SS slag.

2 Experimental

2.1 Sample Preparation and Analysis Method

The chemical compositions selection of synthetic slag refers to that of industrial slag. The components on the basis of mass percentages are 46.67% CaO, 33.33% SiO_2, 8.00% MgO, 6.00% Al_2O_3, 6.00% Cr_2O_3 and 8.00% FeO, respectively. Accurate weighing the components in analysis pure (Sinopharm Chemical Reagent Co., Ltd, Shanghai, China) totals 200g, and FeO is replaced by ferrous oxalate (Sinopharm Chemical Reagent Co., Ltd, Shanghai, China). Then these chemical reagents were fully mixed five times using sieve (φ = 0.5 mm) and evenly put into molybdenum crucible.

In order to ensure completely melting of the sample, the crucible was placed in the isothermal zone in the carbon tube furnace (Power 25KVA) shown in Figure 1. The temperature regime is shown in Figure 2. The heating temperature ranged from 20°C to 1600°C at a rate of 10°C/min and preserved heat for 30 min at 1600°C with high purity N_2 as protective atmosphere. After this operation, the samples were cooled to 1300°C at the cooling rates 1°C/min, 6°C/min and 12°C/min, respectively. The first sampling started at 1580°C, and then sampled per 20°C during the cooling process, the last sampling temperature was 1400°C. The samples were directly quenched by water.

Then the samples for scanning electron microscopy (SEM) were prepared from the resin (HMR4) by XQ-2B, and then grinded, polished and sprayed with gold. Finally, a scanning electron microscope equipped with an

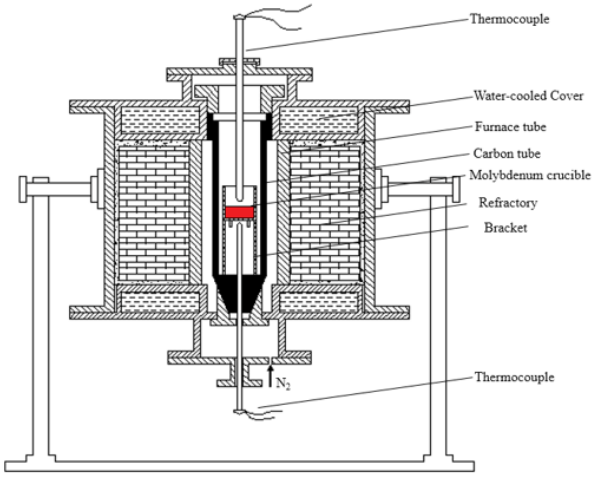

Figure 1: Schematic diagram of carbon tube furnace

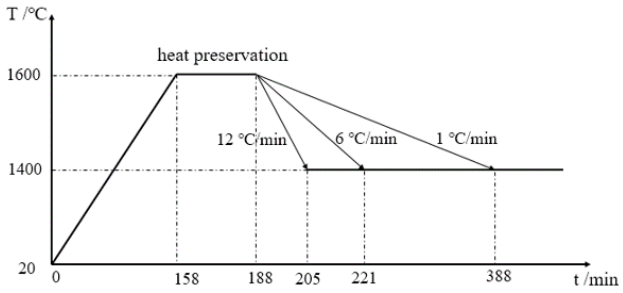

Figure 2: Schematic diagram of temperature regime

energy dispersive spectrometer (SEM-EDS, NanoSEM400, FEI, Hillsboro, OR, US) was used to observe the micromorphology, and an Image-Pro Plus 6.0 (IPP, Media Cybernetics, MD, US) was used to study the variation of spinel crystal size. After grinding the appropriate amount of slag samples, an X-ray diffraction (XRD, X Pert Pro MPD, PANalytica, Almelo, Netherlands) was used to analyze the mineral composition.

2.2 Thermodynamic Simulation

According to Scheil-Gulliver equation, FactSage7.1 (GTT-Technologies, Aachen, Germany) was applied to simulate the phase transformation and precipitation of the spinel phase during solidification of molten slag. The specific setting conditions are shown as follows.

Database: FactPS, FToxide, FSstel;
Compound setting: idea gas, pure solid;
Solution phase setting: FToxid-SLAGA, FToxid-SPINA, FToxid-MeO_A, FToxid-bC_2SA, FToxid-aC_2SA, FToxid-Mel_A.

The FToxid-SLAGA was set as the target phase of Scheil-Gulliver Cooling. The setting temperature was 2000°C and the solidification step was 10°C. The calculation process terminated automatically when the target phase completely disappeared. The results were exported in picture and edited by FactSage7.1.

3 Results and Discussion

The solidification process of CaO-SiO_2-MgO-Al_2O_3-Cr_2O_3-8*wt*%FeO slag system was calculated by FactSage 7.1 in Figure 3, an integrated database computing system in chemical thermodynamics. During the solidification process, the mineral phases such as the spinel crystals, *α*-C2S, merwinite ($Ca_3MgSi_2O_8$) and melilite in turn with the decrease

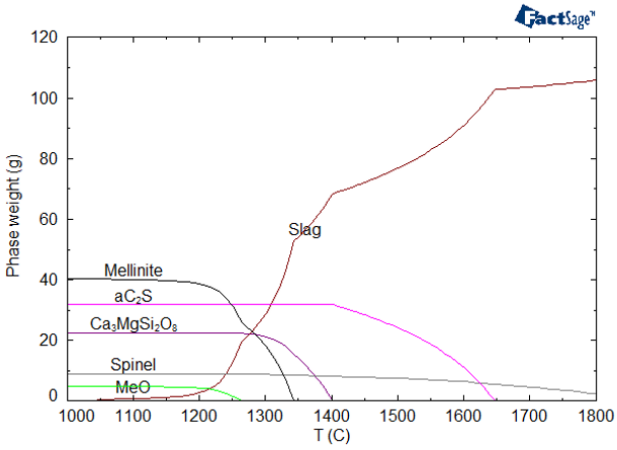

Figure 3: Theoretical analysis of slag solidification process and selection of sampling temperature

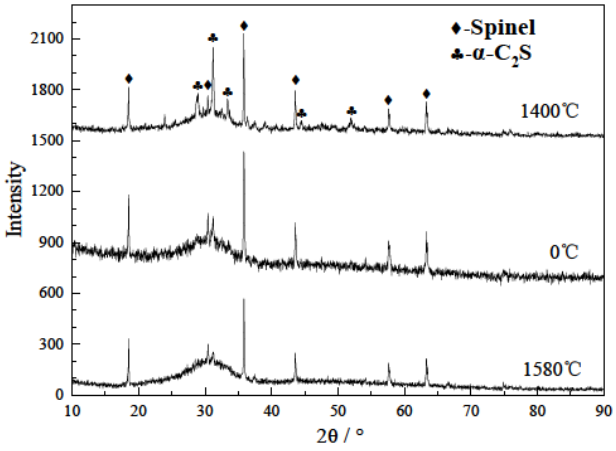

Figure 4: Phase transformation during slag solidification at cooling rate of 1°C/min

of temperature. Among them, the spinel crystal has the highest precipitation temperature, which is higher than 1800°C. The precipitation temperature of *α*-C2S is about 1650°C, and the precipitation amount of *α*-C2S is 10.68 g in per 100g slag at 1600°C. The precipitation temperatures of merwinite ($Ca_3MgSi_2O_8$) and melilite are about 1400°C and 1350°C, respectively.

As shown in Figure 4, the diffraction peaks of spinel crystals always exist and maintain a high intensity at the cooling rate of 1°C/min, indicating that many spinel crystals have been stable at 1600°C. The diffraction peaks of *α*-C2S can be detected at 1500°C, and the intensity of the peaks is stronger at 1400°C, which indicates that *α*-C2S is stable at 1400°C. The XRD patterns in Figure 5 show the diffraction peaks of the samples at 1580°C, 1500°C and 1400°C keep an intensity consistency at the cooling rate of 1°C/min, which means that only the spinel crystals have

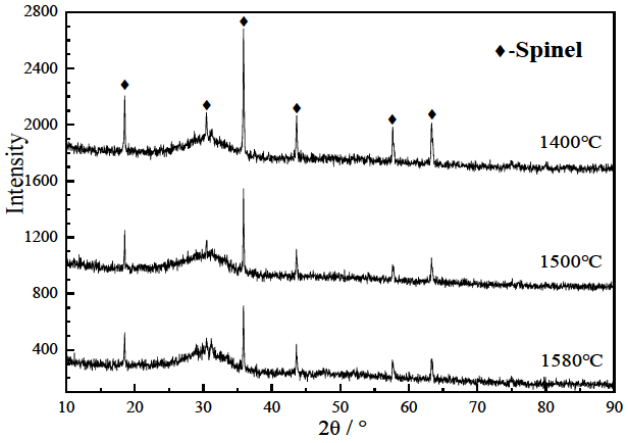

Figure 5: Phase transformation during slag solidification at cooling rate of 12°C/min

diffraction peaks and maintain a high diffraction intensity. These indicate that the larger cooling rate has less influence on the formation of spinel crystals, but inhibits the precipitation of silicates such as α-C2S during the cooling process.

Figure 6 shows the microstructures of the samples at different cooling rates, and the spinel crystals with regular shapes are embedded in the grey silicate matrix. Figure 6 (a), 6 (d) and 6 (g) indicate that the slag consists of only silicate matrix and spinel crystals at high temperature under the three cooling rates, and the effect of cooling intensity begins to appear with the decrease of temperature. As shown in Figure 6(c), 6 (f) and 6 (i), the slag retains a distinct "binary" structure as the cooling rate is 1°C/min at 1400°C. When the cooling rate is 1°C/min, a certain profile of α-C2S begins to appear on the silicate matrix. This is consistent with the observation from the XRD patterns.

Figure 7 and Figure 8 plot the size of spinel crystals counted using IPP 6.0. The size of spinel crystals increases with the solidification process at one cooling rate, the larger the cooling rate, and the larger the size increase. Moreover, no matter what cooling rate is used, the final size of spinel crystals has little difference. It is found that the sizes of spinel crystals cooling at different cooling rates to the same temperature are 11.13 μm and 11.30 μm at 1580°C and 1400°C at the cooling rate of 1°C/min, respectively, and the increase is 1.53%. Whereas the cooling rate is 6°C/min, the sizes are 10.85 μm and 11.6 μm at 1580°C and 1400°C, respectively, and the increase is 3.78%. As compared with the different sampling temperature (1580°C and 1400°C) at the same cooling rate (1°C/min), the sizes of spinel crystals are 10.6 μm and 11.3 μm at 1580°C and 1400°C, respectively, and the increase is 9.45%. The final sizes of spinel crystals increase by only 0.6% and 0.7% at cooling rates of 1°C/min and 6°C/min, respectively, compared with the cooling rates of 12°C/min.

Comparing the effects of different cooling rates on the size of spinel crystals at the same temperature, Figure 8, it is found that the cooling rate has a greater effect on the size of spinel crystals at higher temperature stage, higher 1500°C. The size of spinel crystals increases gradually with the decrease of the cooling rate. Furthermore, the cooling rate has no significant effect on the size of spinel crystals at lower temperature stage, lower then 1500°C. As shown in Figure 7, the size of spinel crystals obtained at 12°C/min cooling rate is 4.0% larger than that at 1°C/min cooling rate at 1580°C, and at 1400°C, the increase rate of spinel crystal size is only 0.6%.

According to the thermodynamic calculation results, spinel crystal is a high temperature precipitation phase, and its precipitation temperature is about 1800°C. Nucleation rate equation gives as follows [19]:

$$I = I_0 \exp\left(-\frac{\Delta G_n^{\circ} + \Delta G_d}{k_B T}\right) \tag{1}$$

where I_0 is the pre-exponential, ΔG_n° is the maximum Gibbs free energy of an atomic group containing N atoms between two temperatures, ΔG_d is the activation energy, and k_B the Boltzmann's constant. Increasing cooling rate results in smaller size and more quantity about nuclei, while the lower liquid temperature leads to lower diffusion rate of solute in the melt. Based on the data of spinel sizes in Figure 7 and Figure 8, the morphologies of spinel crystals are compared in Figure 6 (a), (d) and (g) at different cooling rates. It is found that the number of spinel crystals in these Figures is similar at lower cooling rates, while the number of spinel crystals in Figure 6 (g) pictures is relatively larger. It shows that the spinel crystals have partially nucleated when the cooling begins at 1600°C. With the increase of cooling rate, the temperature of maximum nucleation rate increases due to the activation energy term. This means that the maximum nucleation rate under this composition reaches when the cooling rate is greater than or equal to 12°C/min.

The formation of spinel crystals can be divided into three stages. Firstly, the formation of spinel nuclei. Secondly, the diffusion of solute components in melt, and finally, the adsorption and escape of atoms at the interface between spinel crystals and melt. The crystal growth rate equation give [20]:

$$V = Jv' = v' J_0^{+} exp\left(-\frac{Q}{RT}\right) \alpha \left(\frac{\Delta T}{T}\right) f\,[hk] \tag{2}$$

where $\alpha = \Delta H_f / RT_f$, which is dimensionless entropy, v' is the atomic volume, $f\,[hk]$ the crystallographic factor.

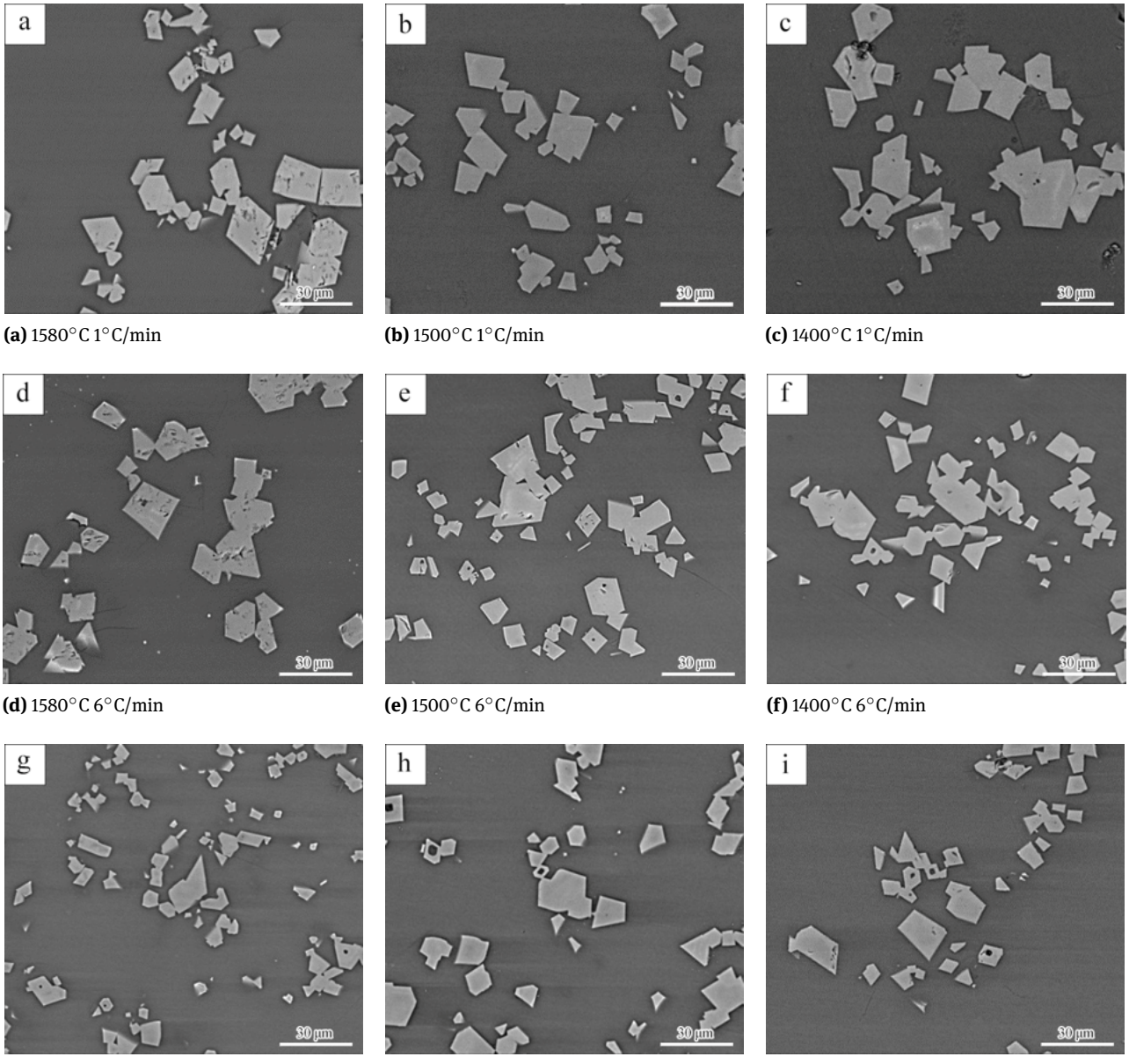

(a) 1580°C 1°C/min **(b)** 1500°C 1°C/min **(c)** 1400°C 1°C/min

(d) 1580°C 6°C/min **(e)** 1500°C 6°C/min **(f)** 1400°C 6°C/min

(g) 1580°C 12°C/min **(h)** 1500°C 12°C/min **(i)** 1400°C 12°C/min

Figure 6: Microstructure of the samples

In the first order approximation, the growth rate of crystals is a linear function of undercooling, and the growth rate of crystals depends mainly on the diffusion of solutes. As shown in Figure 6 (a), it is considered that the solutes in the local region are uniformly distributed. As a crystal grown with a single nucleus, the faster the cooling rate is, the steeper the solute concentration gradient is, and the faster the growth rate is. However, the solubility of the solute boundary layer in the nucleus is less than that in the Figure 6 (a) or Figure 6 (d) due to the larger number of nucleus. Therefore, the size of spinel crystal is the smallest and the number is the largest at 12°C/min. As the cooling rate is 1°C/min, the maximum nucleation is completed near 1580°C. Because of the slower cooling rate, long holding time, relatively slow growth rate, gently solubility gradient. So the maximum size of spinel crystal in Figure 6 (a) is smaller than that in Figure 6 (b) or Figure 6 (c), while the crystal size in Figure 6 (b) or Figure 6 (c) is basically similar. The results show that the solute diffusion is uniform at 1°C/min cooling rate, which is beneficial to the growth of spinel crystal as a whole. Similarly, when the cooling rate is 6°C/min and 12°C/min, the maximum size of the crystals

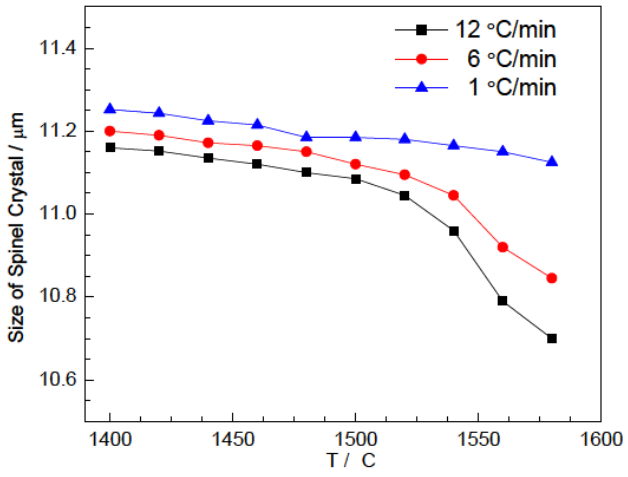

Figure 7: Variation of spinel crystal size during slag solidification

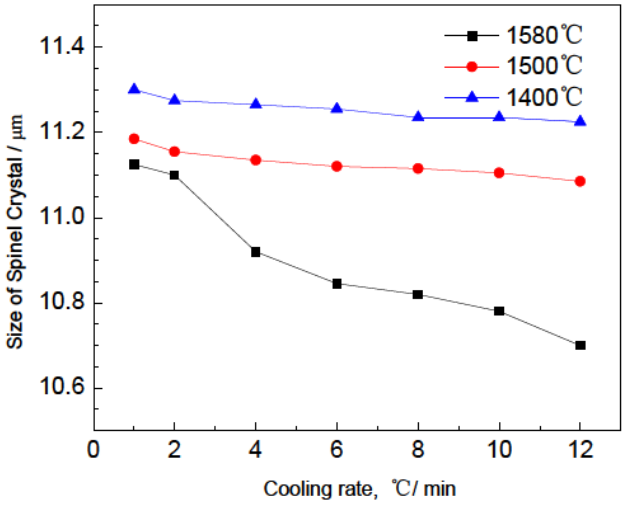

Figure 8: Effect of cooling rate on spinel crystal size

at 1400°C to 1500°C is not much different, indicating that the crystallization process has been completed in the temperature range from 1400°C to 1500°C and that the cooling rate has little effect on the grain size of the spinel crystals, but more importantly on the nucleation.

4 Conclusion

The effect of cooling rate on crystallization behavior in CaO-SiO_2-MgO-Cr_2O_3 based slag system has been determined by using the FactSage 7.1, SEM-EDS, IPP 6.0 and XRD. The results of the present work can be summarized as follows.

1. The spinel crystal has a high precipitate temperature, which is higher than 1800°C. The main precipitates are α-C2S, merwinite ($Ca_3MgSi_2O_8$) and melilite from FactSage 7.1.
2. The cooling rates have little effect on the particle size of spinel crystals, but a great influence on the precipitation of silicates such as α-C2S. The spinel crystals and α-C2S can be formed and precipitated during cooling process when the cooling rate is 1°C/min, but only the spinel crystals can be precipitated when cooling rate is 12°C/min.
3. The size of the spinel crystals obtained at 12°C/min cooling rate is 4.0% larger than that at 1°C/min cooling rate at 1580°C, and at 1400°C, the increase rate of the spinel crystal size is only 0.6%. In general, the cooling rate has little effect on the growth of spinel crystals, and a slightly stronger effect on the size of spinel crystals at high temperature (greater than 1500°C) than at low temperature (less than 1500°C).
4. The chromium in silicate phase is easy to leach with the dissolution of the silicate phase. Hence, the formation of silicate phase should be controlled. It is suggested that the cooling rate of the SS slag in industrial treatment should be greater than or equal to 12°C/min, duo to the trend of cooling rate on crystals formation.

Acknowledgement: The authors would like to thank the anonymous reviewers for their constructive comments and suggestions. The work was supported by the National Natural Science Foundation of China (No. 51974210), the Hubei Provincial Natural Science Foundation (No. 2019CFB697), the China Postdoctoral Science Foundation (No. 2014M562073), and the State Key Laboratory of Refractories and Metallurgy.

References

[1] Rosales, J., M. Cabrera, and F. Agrela. Effect of stainless steel slag waste as a replacement for cement in mortars. Mechanical and statistical study. Construction & Building Materials, Vol. 142, 2017, pp. 444–458.

[2] Y.B. Zong, Y. Li, and D.Q. Cang. Experimental Study on Stainless Steel Slag Used in Ceramic Making. Advanced Materials Research, Vol. 156, 2010, pp. 758–760.

[3] Estokova, A., L. Palascakova, and M. Kanuchova. Study on Cr(VI) Leaching from Cement and Cement Composites. International Journal of Environmental Research and Public Health, Vol. 15, 2018, Article id. 824.

[4] C. Casalegno, O. Schifanella, E., Zennaro, S. Marroncelli, and R. Briant. Collate Literature Data on Toxicity of Chromium (Cr) and Nickel (Ni) in Experimental Animals and Humans. European Food Safety Authority, Supporting Publication, EN-478, 2015, pp.

1–287.

[5] Cheng, S., Z. Shui, R. Yu, X. Zhang, and S. Zhu. Durability and environment evaluation of an eco-friendly cement-based material incorporating recycled chromium containing slag. Journal of Cleaner Production, Vol. 185, 2018, pp. 23–31.

[6] Dong, Y. B., Y. Liu, and H. Lin. Leaching behavior of V, Pb, Cd, Cr, and As from stone coal waste rock with different particle sizes. International Journal of Minerals Metallurgy and Materials, Vol. 15, No. 8, 2018, pp. 861–870.

[7] Kayhanian, M., A. Vichare, P. G. Green, and J. Harvey. Leachability of dissolved chromium in asphalt and concrete surfacing materials. Journal of Environmental Management, Vol. 90, No. 11, Aug. 2009, pp. 3574–3580.

[8] Tsomondo, M. B. C., and D. J. Simbi. Kinetics of chromite ore reduction from MgO-CaO-SiO_2-FeO-Cr_2O_3-Al_2O_3 slag system by carbon dissolved in high carbon ferrochromium alloy bath. Ironmaking & Steelmaking, Vol. 29, No. 1, 2002, pp. 22–28.

[9] Gutiérrez Paredes, J., A. Romero Serrano, G. Plascencia Barrera, M. Vargas Ramírez, B. Zeifert, and V. Arredondo Torres. Chromium Oxide Reduction from Slag by Silicon and Magnesium. Steel Research International, Vol. 67, No. 11, 2005, pp. 764–768.

[10] Adamczyk, B., R. Brenneis, C. Adam, and D. Mudersbach. Recovery of Chromium from AOD-Converter Slags. Steel Research International, Vol. 81, No. 12, 2010, pp. 1078–1083.

[11] Lin, Y. , K.-C. Chou, P. Scheller, and Q. Shu. Reduction of Synthetic Stainless Steel Slags by Aluminium. Ironmaking & Steelmaking, Vol. 46, 2019, pp. 81–88.

[12] Sheen, Y., H. Wang, and T. Sun. A study of engineering properties of cement mortar with stainless steel oxidizing slag and reducing slag resource materials. Construction & Building Materials, Vol. 40, 2013, pp. 239–245.

[13] Zeng, Q., J. Li, and Q. Mou. H. Zhu, and Z. Xue, JOM-US., Vol. 71, 2019, pp. 2331–2337.

[14] Long-hu. Cheng-jun, Q. Zhao, and M.-F. Jiang, J. Iron. Steel Research, Vol. 24, 2017, pp. 258–265.

[15] Pillay, K., H. von Blottnitz, and J. Petersen. Ageing of chromium(III)-bearing slag and its relation to the atmospheric oxidation of solid chromium(III)-oxide in the presence of calcium oxide. Chemosphere, Vol. 52, No. 10, Sep. 2003, pp. 1771–1779.

[16] H. Q. Zhao, Q. I. Yuan-Hong, Y. L. Shi, N. A, Xian-Zhao, and H. L. Feng, J. Iron. Steel Research, Vol. 20, 2013, pp. 26–30.

[17] Kriskova, L., Y. Pontikes, L. Pandelaers, Ö. Cizer, P. T. Jones, K. Van Balen, and B. Blanpain. Effect of High Cooling Rates on the Mineralogy and Hydraulic Properties of Stainless Steel Slags. Metallurgical and Materials Transactions. B, Process Metallurgy and Materials Processing Science, Vol. 44, No. 5, 2013, pp. 1173–1184.

[18] Li, W. and X. Xue. Effects of Silica Addition on Chromium Distribution in Stainless-steel Slag. Ironmaking & Steelmaking, Vol. 45, 2018, pp. 929–936.

[19] Christian, J. W. The Theory of Transformations in Metals and Alloys. Materials Today, Vol. 6, No. 3, 2003, p. 53.

[20] Jackson, K. A. On the Theory of Crystal Growth: the Fundamental Rate Equation. Journal of Crystal Growth, Vol. 5, No. 1, 1969, pp. 13–18.